PHYSICAL REVIEW B VOLUME 60, NUMBER 14 1 OCTOBER 1999-II

Neutron diffraction from thermally fixed gratings in photorefractive lithium niobate crystals

I. Nee, K. Buse, and F. Havermeyer
Fachbereich Physik, Universität Osnabrück, D-49069 Osnabrück, Germany

R. A. Rupp and M. Fally
Institut für Experimentalphysik, Universität Wien, A-1090 Wien, Austria

R. P. May
Institut Laue-Langevin, F-38042 Grenoble Cedex, France

(Received 14 July 1999)

Iron-doped lithium niobate crystals are illuminated with a sinusoidal light pattern (period length 374 nm) at a temperature of about 180 °C. Electrons are redistributed and ions drift in the electronic space-charge pattern (''thermal fixing''). At room temperature the ions are almost immobile. A density grating (space-charge field plus inverse-piezoelectric effect) and the ionic grating yield a refractive-index modulation for neutrons (''photorefractive effect''). Neutrons (wavelength 1.39 nm) are diffracted from this grating with an efficiency up to 1.2×10^{-3}. Usually hydrogen ions form the ionic grating. The ions responsible for charge compensation in dehydrated crystals have a much smaller coherent neutron-scattering length and might be identified as lithium. [S0163-1829(99)50738-8]

Inhomogeneous illumination redistributes electrons in iron-doped lithium niobate crystals ($LiNbO_3$), space-charge fields build up and these fields modulate the refractive index for light via the electro-optic effect. Iron ions in the valence states $2+$ and $3+$ are sources and traps of the electrons,[1] and the bulk-photovoltaic effect is the dominant charge-driving force.[2] Photorefractive $LiNbO_3$ crystals find more and more applications,[3] e.g., outstanding wavelength filters,[4] promising wavelength-division multiplexers,[5,6] and volume holographic memories[7] were fabricated.

Homogeneous illumination redistributes the electrons back and erases the stored patterns. Thermal fixing, i.e., heating of the crystals during or after recording, is an approach to overcoming this problem.[8] The process relies on the fact that ions become mobile at temperatures of about 180 °C. They move and compensate for the electron redistribution. Supposing that we have enough movable ions, the charge redistribution continues until the bright regions are depleted (no more filled traps Fe^{2+}) or until the dark regions are saturated (no more empty traps Fe^{3+}). Cooling to room temperature decreases the mobility of the ions by several orders of magnitude. Homogeneous irradiation with light yields modulated currents because the concentrations of Fe^{2+} and Fe^{3+} ions are spatially modulated.[9] This step is called ''development'' because the hologram is revealed. Large space-charge fields build up. Electronic drift currents in these space-charge fields compensate the photovoltaic currents and no more electrons are redistributed. As a consequence, the Fe^{2+} and Fe^{3+} concentration patterns cannot be erased by light, and the corresponding space-charge fields modulate the refractive-index permanently.

Spectroscopic investigations revealed that protons (hydrogen ions, OH^- bonds) are mobile and form the compensating grating, if enough protons are available.[9,10] However, thermal fixing is possible also in dehydrated crystals[9] but it is not known so far which ions move. One of the possible explanations is that Li ions migrate, because congruently melting $LiNbO_3$ (melt and crystal have the same composition) is not stoichiometric and has a Li^+ deficit of about 4%.[11–13] Furthermore, Li ions are rather small and Li^+ hopping conduction may occur. Identification of the compensating ions and measurement of their mobility are essential for an estimation of the lifetime of thermally fixed holograms. A couple of years is obtained with hydrogen fixing,[14,15] but the aim is to achieve much higher lifetimes, maybe thousands of years for archival data storage.

Here we report a new approach for investigation of the charge-transport processes: Diffraction of neutrons from thermally fixed gratings. The refractive index for neutrons depends on the density of nuclei and on the types of isotopes involved, i.e., on their coherent scattering lengths. Two kinds of gratings can influence the neutrons: (i) A modulated density of the host material ($LiNbO_3$) which occurs because of the electric space-charge fields and the inverse-piezoelectric effect (electro-neutron-optic effect);[16] (ii) an ionic grating.

The strategy is to measure the diffraction efficiency of neutrons, to separate the effects arising from the two gratings mentioned above, and to deduce the coherent scattering length per ion in order to identify the ions with the help of this parameter, which varies for all elements and isotopes. Apart from this rather applied background it is fascinating in itself to check whether it is possible to diffract neutrons from light-induced and thermally fixed gratings. In the case of high efficiencies, neutron-optical components (beam splitters, mirrors, interferometers, and switches) might be fabricated by thermal fixing in $LiNbO_3$. Recently, Schellhorn *et al.* succeeded in preparing an interferometer for cold neutrons which utilizes three holographic gratings recorded in poly(methylmethacrylate).[17] One of the exciting questions is whether it is feasible to realize such an instrument or even more advanced devices with thermally fixed gratings in $LiNbO_3$.

We investigate two congruently melting $LiNbO_3$ crystals. They were grown by Deltronic Crystal Ind. and doped by

TABLE I. Notation, dimensions (B: length along the propagation direction of recording light and neutrons; C: length of the polar axis), ion concentrations ($c_{Fe}=c_{Fe^{2+}}+c_{Fe^{3+}}$, overall iron concentration; $c_{Fe^{2+}}$, concentration of Fe^{2+} ions; $c_{Fe^{3+}}$, concentration of Fe^{3+} ions; c_{OH^-}, concentration of OH^- ions), and annealing treatment (Vac., Vacuum; h, humid; d, dry) of the samples used.

Notation	DT2–27	DT2–28
Dimensions $(A\times B\times C)$ [mm^3]	$9.1\times 2.9\times 10.3$	$9.2\times 2.9\times 10.3$
c_{Fe} [10^{24} m^{-3}]	51	51
$c_{Fe^{2+}}$[10^{24} m^{-3}]	1.8	2.5
$c_{Fe^{2+}}/c_{Fe^{3+}}$	0.037	0.052
c_{OH^-}[10^{24} m^{-3}]	5.64	0.47
Annealing	6 h, h$-O_2$,1000 °C 2 h, h$-$Ar,900 °C	36 h, Vac., 1000 °C 2 h, d$-O_2$,1000 °C 1 h, d$-O_2$,950 °C

adding 0.138 wt. % Fe_2O_3 to the melt. No specially selected isotopes were used, i.e., about 92.5% ^{7}Li and 7.5% ^{6}Li are present. Two samples were prepared and relevant crystal parameters can be found in Table I. Thermal annealing was performed to adjust the concentration of OH^-. Sample DT2–27 was annealed in humid gases (the gases enter the annealing oven through a water bath) while sample DT2–28 was annealed in dry atmosphere. The concentrations of Fe^{2+} and of OH^- ions were deduced from absorption measurements,[1,18,19] (charge transfer from Fe^{2+} to the conduction band yields an absorption at 477 nm and excitation of OH^- vibrations occurs at 2870 nm). Sample DT2–27 contains more OH^- than Fe^{2+}, i.e., all Fe^{2+} patterns can be compensated completely by moving hydrogen ions. However, the OH^- concentration in the crystal DT2–28 is much too small to compensate for strongly modulated Fe^{2+} patterns.

Holographic gratings were recorded at a crystal temperature of 180 °C by interference of two plane waves [wavelength of 514.5 nm, ordinary polarization, grating vector aligned almost along the polar crystal axis (deviation less than 2°), period length of the grating $\Lambda=374$ nm, recording beam intensities of 820 W/m^2 and 440 W/m^2 (DT2–27) and 600 W/m^2 and 450 W/m^2 (DT2–28), and recording times of 90 min (DT2-27) and 130 min (DT2-28)]. The setup is actively stabilized against mechanical vibrations to ensure stable holographic recording.[20] Afterwards, the crystals are cooled to room temperature and illuminated homogeneously with white light of an incandescent lamp (150 W/m^2, for 60 min).

An angular-dependent read-out of the developed gratings is performed with light of a HeNe laser (wavelength of 632.8 nm, ordinary polarization). The results are very well described by the solution of the coupled-wave equations[21] and fits to the data yield the amplitudes of the refractive index gratings $\Delta n_{red}=(2.2\pm 0.2)\times 10^{-4}$ (DT2–27) and $\Delta n_{red}=(2.1\pm 0.4)\times 10^{-4}$ (DT2–28). The expected saturation value for crystals with this iron content and for *fully* modulated Fe^{2+} patterns is $\Delta n_{red}=4.8\times 10^{-4}$.[22,23] This yields for the concentration amplitudes of the spatial Fe^{2+} gratings the result $\Delta c_{Fe^{2+}}=[(2.2\pm 0.2)/4.8]c_{Fe^{2+}}=(0.83\pm 0.08)$ 10^{24}m^{-3} (DT2–27), and $\Delta c_{Fe^{2+}}=[(2.1\pm 0.4)/4.8]c_{Fe^{2+}}=(1.1\pm 0.2)\times 10^{24}$ m^{-3} (DT2–28). Fully modulated Fe^{2+} patterns, i.e., $\Delta c_{Fe^{2+}}=c_{Fe^{2+}}$, can be obtained by longer recording. Anyhow, we also know from the measured $\Delta c_{Fe^{2+}}$ the amplitudes of the ionic gratings, $\Delta c_{ions}=\Delta c_{Fe^{2+}}/Z$, where Z is the number of the effective unit charges per ion ($Z=1$ for OH^- which has the effective charge $+e$). The amplitudes E_{sc} of the space-charge fields in the developed state are also known because of the relation $\Delta n(\lambda)=-(1/2)n(\lambda)^3 r(\lambda)E_{sc}$, where $n=2.28$ (Ref. 24) is the refractive index, and $r=10$ pm/V (Ref. 24) the electro-optic coefficient for red light (wavelength $\lambda=632.8$ nm). We get $E_{sc}=(3.7\pm 0.4)\times 10^6$ V/m (DT2–27) and $E_{sc}=(3.5\pm 0.8)\times 10^6$ V/m (DT2–28).

Neutron-diffraction experiments were performed at the Institut Laue-Langevin (ILL) in Grenoble, France with the small-angle neutron-scattering instrument D22 (Ref. 25) (128×128 detector matrix placed 18 m behind the sample). The relative sensitivity of each detector element (detector pixel, 7×7 mm^2) is calibrated prior to the measurements with an isotropic scatterer. Cold neutrons [wavelength $\lambda_n=1.39$ nm, wavelength distribution of 10%, Cd-collimation diaphragms of 15×15 mm^2 (input) and 8×8 mm^2 (output) with a distance of 19.1 m, and a neutron flux of 47 200 neutrons/s] are employed. The crystal is placed in the beam and a peak of diffracted neutrons is clearly observed on the detector matrix after adjustment of the Bragg angle. The neutron background at the same detector elements is measured, too, by turning the crystal out of the Bragg angle. The difference of the signals yields the number of diffracted neutrons, and the diffraction efficiency η is determined, i.e., the number of diffracted neutrons divided by the sum of the transmitted and diffracted neutrons. Typical measurements take between 8 and 120 min. The crystals are rotated with the help of a mechanical rotation stage and Fig. 1 shows the angular dependence of the diffraction efficiencies in the developed state. Bragg peaks on both sides of the symmetric position are clearly observed. The measured Bragg angle of about $\Theta_B=(1.8\pm 0.1)$ mrad agrees excellently with the expected one [$\sin\Theta_B=\lambda_n/(2\Lambda)$ yields $\Theta_B=(1.86\pm 0.05)$ mrad], confirming that the neutrons are indeed diffracted from the grating. The obtained diffraction efficiencies are rather high and reach up to 2.0×10^{-4} (DT2–27) and 1.1×10^{-4} (DT2–28). The measurement accuracy depends on the integration time and error bars are shown directly in the figures. The neutrons are partly incoherent. This yields a broadening of the Bragg peaks and a reduction of the peak values.[21] Consideration of this effect[16] enables computation of coherent diffraction efficiencies of $\eta_{coh}=1.2\times 10^{-3}$ (DT2–27) and $\eta_{coh}=0.6\times 10^{-3}$ (DT2–28), i.e., these efficiencies are expected for a perfectly coherent neutron beam. As pointed out above, two effects may contribute to neutron diffraction in the developed state: (i) Interaction of the space-charge field with the inverse piezoelectric effect (electro-neutron-optic effect) and (ii) the ionic gratings.

The space-charge fields were erased by heating the sample (DT2–27 at 100 °C for 45 min; DT2–28 at 110 °C

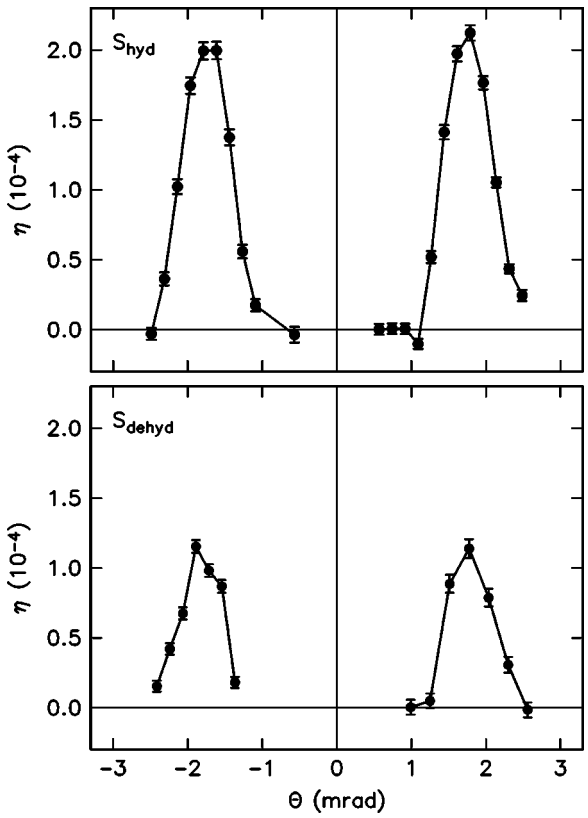

FIG. 1. Neutron diffraction efficiency η versus angle Θ between the propagation direction of the neutron beam and the grating normal for the samples DT2–27 (top) and DT2–28 (bottom) in the *developed* state (space-charge fields are present). The symbols correspond to the measured data and the solid lines are guides to the eye. The error bars represent the standard deviation.

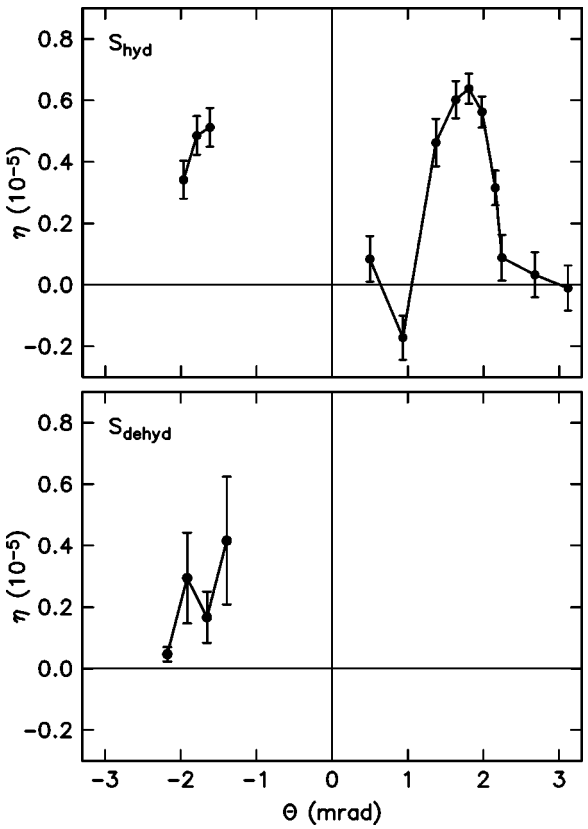

FIG. 2. Neutron diffraction efficiency η versus angle Θ between the propagation direction of the neutron beam and the grating normal for the samples DT2–27 (top) and DT2–28 (bottom) in the *erased* state (concentration gratings, but no space-charge fields are present). The symbols correspond to the measured data and the solid lines are guides to the eye. The error bars represent the standard deviation.

for 105 min). A negligible amount of the ions moves back, but this movement is sufficient to compensate completely the previously developed space-charge fields. Angular dependent measurements of the neutron-diffraction efficiency are once more performed and Fig. 2 shows the results. The diffraction efficiencies dropped strongly for both samples. However, the crystals exhibit a different behavior: Sample DT2–27 still shows a Bragg peak ($\eta_{\mathrm{coh}}=3.6\times10^{-5}$) while no more diffracted neutrons can be detected for the dehydrated sample DT2–28 ($\eta_{\mathrm{coh}}<1.8\times10^{-5}$).

The diffraction efficiency can be written as (Ref. 21)

$$\eta_{\mathrm{coh}}=\left(\frac{\pi B\Delta n_{\mathrm{n}}}{\lambda_{\mathrm{n}}\cos\Theta_{\mathrm{B}}}\right)^2, \tag{1}$$

where B is the thickness of the sample and Δn_{n} is the change of the refractive index for neutrons. According to this relation, our refractive index gratings have in the developed state (with space-charge fields) the amplitudes $|\Delta n_{\mathrm{n}}|=5.3\times10^{-9}$ (DT2–27) and $|\Delta n_{\mathrm{n}}|=3.7\times10^{-9}$ (DT2–28). The strong decrease of the efficiencies after erasure of the space-charge fields shows that the electro-neutron-optic effect strongly dominates in the developed state.

Thermal erasure of the space-charge fields decreases the grating amplitudes to $\Delta n_{\mathrm{n}}=0.92\times10^{-9}$ (DT2–27) and $\Delta n_{\mathrm{n}}<0.65\times10^{-9}$ (DT2–28), which are supposed to originate from the ionic gratings only. From the above analysis we know that in sample DT2–27 a grating of hydrogen ions is present [concentration amplitude $\Delta c_{\mathrm{OH}^-}=\Delta c_{\mathrm{ions}}=(0.83\pm0.08)\times10^{24}\ \mathrm{m}^{-3}$]. This should yield a modulation of the refractive index for neutrons of about $\Delta n_{\mathrm{n}}=\Delta n_{\mathrm{ionic}}=-[\lambda_{\mathrm{n}}^2/(2\pi)]b_{\mathrm{c}}\Delta c_{\mathrm{ions}}$,[26] where b_{c} is the coherent scattering length. A $b_{\mathrm{c}}=-3.74$ fm for ^{1}H (Ref. 27) yields $\Delta n_{\mathrm{n}}=(0.95\pm0.1)\times10^{-9}$. This agrees excellently with the measured value. The dehydrated sample DT2–28 exhibits a $\Delta n_{\mathrm{n}}<0.65\times10^{-9}$, and $\Delta c_{\mathrm{ions}}=(1.1\pm0.2)\times10^{24}\ \mathrm{m}^{-3}$ yield $|b_{\mathrm{c}}|\lesssim1.9$ fm, supposing that each ion carries one effective unit charge ($Z=1$). Lithium of the natural isotopic composition has an exceptionally small b_{c} of only -1.9 fm.[27] This indicates that probably the explanation of thermal fixing in dehydrated crystals via lithium hopping conduction is valid. However, further experiments are required to accomplish a full understanding of the role of Li ions in the process of thermal fixing.

We may write in the developed state (with space-charge fields) $\Delta n_{\mathrm{n}}=\Delta n_{\text{electro-optic}}+\Delta n_{\mathrm{ionic}}$ with $\Delta n_{\text{electro-optic}}=-(1/2)r_{\mathrm{n}}E_{\mathrm{sc}}$. Neutron-electro-optic and ionic gratings can be in phase or 180° out of phase, depending on the signs of the material parameters involved (the sign of the neutron-electro-optic coefficient r_{n}, the sign of the coherent neutron-scattering length b_{c}, ...). Other phase shifts are not expected for recording in iron-doped $LiNbO_3$ crystals.[28] Thus the gratings can either compensate or amplify each

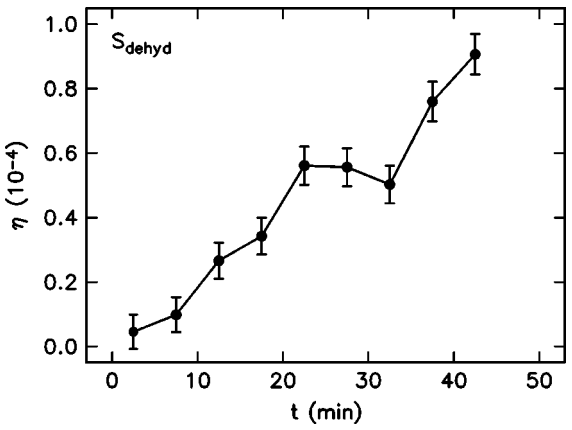

FIG. 3. Evolution of the neutron diffraction efficiency η for the sample DT2–27 in one of the Bragg peaks ($\Theta \approx 1.8$ mrad) during development with white incandescent light. The symbols correspond to the measured data and the solid lines are guides to the eye. The error bars illustrate the standard deviation.

other (different or equal signs of $\Delta n_{\text{electro-optic}}$ and Δn_{ionic}). Considering $\Delta n_n = 5.3\times10^{-9}$, $\Delta n_{\text{ionic}} = 0.92\times10^{-9}$, and $E_{sc} = (3.7\pm0.4)\times10^6$ (DT2–27) we get $r_n = [(2.4-3.4)\pm0.5]$ fm/V, and considering $\Delta n_n = 3.7\times10^{-9}$, $\Delta n_{\text{ionic}} = 0.65\times10^{-9}$, and $E_{sc} = (3.5\pm0.8)\times10^6$ (DT2–28) we get $r_n = [(1.7-2.5)\pm0.8]$ fm/V. All results together yield for the electro-neutron-optic coefficient $r_n = (2.6\pm0.7)$ fm/V.

Heating erases the space-charge fields, but the concentration patterns are almost unchanged. This can be verified by Fig. 3, which shows the evolution of the neutron-diffraction efficiency η in the Bragg peak during homogeneous illumination with white incandescent light. The increase of η during the development can be nicely observed.

A further threefold increase of the space-charge fields up to $E_{sc} = 10\times10^6$ V/m by using larger recording times is realistic, but fields above this threshold cannot be achieved because of electric break-downs.[9] Thus electro-neutron-optic $|\Delta n_n| = |(1/2) r_n E_{sc}|$ values up to 1.3×10^{-8} can be expected. Furthermore, samples of larger thickness can be employed and a thickness of $B = 1$ cm is still a reasonable value. Considering Eq. (1) one sees that an increase of η_{coh} from the obtained $\eta_{\text{coh}} = 1.2\times10^{-3}$ up to $\eta = 0.1$ is feasible.

In conclusion, neutrons can be diffracted from thermally fixed gratings in iron-doped lithium niobate crystals. Coherent diffraction efficiencies up to 1.2×10^{-3} are reached. The electro-neutron-optic effect (space-charge fields interact with the inverse-piezoelectric effect) yields the major contribution to the neutron refractive index grating. Refractive index changes caused by ionic compensation gratings are at least one order of magnitude smaller. Experiments with undeveloped crystals indicate that ions with a small coherent neutron-scattering length, maybe lithium, are responsible for charge compensation in dehydrated crystals.

We thank S. Breer for fruitful discussions. Financial support from Volkswagen-Stiftung (Project No. I/73920) and attribution of neutron beam time by the ILL are gratefully acknowledged.

[1] H. Kurz, E. Krätzig, W. Keune, H. Engelmann, U. Gonser, B. Dischler, and A. Räuber, Appl. Phys. **12**, 355 (1977).
[2] A.M. Glass, D. von der Linde, and T.J. Negran, Appl. Phys. Lett. **25**, 233 (1974).
[3] P. Günter and J.-P. Huignard, *Topics in Applied Physics: Photorefractive Materials and Their Applications II*, Topics Appl. Phys. Vol. 62 (Springer, Berlin, 1989).
[4] V. Leyva, G.A. Rakuljic, and B. O'Conner, Appl. Phys. Lett. **65**, 1079 (1994).
[5] S. Breer and K. Buse, Appl. Phys. B: Lasers Opt. **66**, 339 (1998).
[6] S. Breer, H. Vogt, I. Nee, and K. Buse, Electron. Lett. **34**, 2419 (1999).
[7] I. McMichael, W. Christian, D. Pletcher, T.Y. Chang, and J.H. Hong, Appl. Opt. **35**, 2375 (1996).
[8] J.J. Amodei and D.L. Staebler, Appl. Phys. Lett. **18**, 540 (1971).
[9] K. Buse, S. Breer, K. Peithmann, S. Kapphan, M. Gao, and E. Krätzig, Phys. Rev. B **56**, 1225 (1997).
[10] H. Vormann, G. Weber, S. Kapphan, and E. Krätzig, Solid State Commun. **40**, 543 (1981).
[11] B.C. Grabmaier, W. Wersing, and W. Koestler, J. Cryst. Growth **110**, 339 (1991).
[12] N. Iyi, K. Kitamura, F. Izumi, J.K. Yamamoto, T. Hayashi, H. Asano, and S. Kimura, J. Solid State Chem. **101**, 340 (1992).
[13] N. Zotov, H. Boysen, J. Schneider, and F. Frey, Mater. Sci. Forum **166-169**, 631 (1994).
[14] A. Yariv, S. Orlov, G. Rakuljic, and V. Leyva, Opt. Lett. **20**, 1334 (1995).
[15] A. Yariv, S.S. Orlov, and G.A. Rakuljic, J. Opt. Soc. Am. B **13**, 2513 (1996).
[16] F. Havermeyer, R. A. Rupp, and R. P. May, Appl. Phys. B: Lasers Opt. **68**, 995 (1999).
[17] U. Schellhorn, R.A. Rupp, S. Breer, and R.P. May, Physica B **234-236**, 1068 (1997).
[18] E. Krätzig and R. Orlowski, Appl. Phys. **15**, 133 (1978).
[19] S. Kapphan and A. Breitkopf, Phys. Status Solidi A **133**, 159 (1992).
[20] S. Breer, K. Buse, K. Peithmann, H. Vogt, and E. Krätzig, Rev. Sci. Instrum. **69**, 1591 (1998).
[21] H. Kogelnik, Bell Syst. Tech. J. **48**, 2909 (1969).
[22] K. Peithmann, A. Wiebrock, and K. Buse, Appl. Phys. B: Lasers Opt. **68**, 777 (1999).
[23] S. Fries and S. Bauschulte, Phys. Status Solidi A **125**, 369 (1991).
[24] *Ferroelectrics amd Related Substances*, edited by K.-H. Hellwege, Landolt-Börnstein New Series, Group III, Vol. 16 (Springer-Verlag, Berlin, 1981).
[25] *Guide to Neutron Research Facilities at the ILL* (The Yellow Book), edited by H.G. Buettner, E. Lelievre-Berna, and F. Pinet (Institut Laue-Langevin, Grenoble, France, 1997).
[26] H. Dachs, *Topics in Current Physics—Neutron Diffraction* (Springer, Berlin, 1978).
[27] V.F. Sears, *Methods of Experimental Physics* (Academic, New York, 1986), Vol. 23, Pt. A, p. 521–549.
[28] R. Matull and R.A. Rupp, J. Phys. D **21**, 1556 (1988).